Critical behavior of the two-dimensional icosahedron model

Hiroshi Ueda,[1] Kouichi Okunishi,[2] Roman Krčmár,[3] Andrej Gendiar,[3] Seiji Yunoki,[1,4,5] and Tomotoshi Nishino[6]
[1]*Computational Materials Science Research Team, RIKEN Advanced Institute for Computational Science (AICS), Kobe 650-0047, Japan*
[2]*Department of Physics, Niigata University, Niigata 950-2181, Japan*
[3]*Institute of Physics, Slovak Academy of Sciences, SK-845 11, Bratislava, Slovakia*
[4]*Computational Condensed Matter Physics Laboratory, RIKEN, Wako, Saitama 351-0198, Japan*
[5]*Computational Quantum Matter Research Team, RIKEN Center for Emergent Matter Science (CEMS), Wako, Saitama 351-0198, Japan*
[6]*Department of Physics, Graduate School of Science, Kobe University, Kobe 657-8501, Japan*
(Received 5 September 2017; published 11 December 2017)

In the context of a discrete analog of the classical Heisenberg model, we investigate the critical behavior of the icosahedron model, where the interaction energy is defined as the inner product of neighboring vector spins of unit length pointing to the vertices of the icosahedron. The effective correlation length and magnetization of the model are calculated by means of the corner-transfer-matrix renormalization group (CTMRG) method. A scaling analysis with respect to the cutoff dimension m in CTMRG reveals a second-order phase transition characterized by the exponents $\nu = 1.62 \pm 0.02$ and $\beta = 0.12 \pm 0.01$. We also extract the central charge from the classical analog of entanglement entropy as $c = 1.90 \pm 0.02$, which cannot be explained by the minimal series of conformal field theory.

DOI: 10.1103/PhysRevE.96.062112

I. INTRODUCTION

Statistical models with short-range interactions on two-dimensional (2D) regular lattices exhibit no spontaneously symmetry breaking at finite temperatures, if the symmetry in local degrees of freedom is continuous [1]. The classical ferromagnetic XY model is a typical example, which has $O(2)$ symmetry, where the thermal average of the magnetization is zero at finite temperature. An introduction of discrete nature to local degrees of freedom then induces an order-disorder transition at low temperatures, where the universality class is dependent on the type of discretization. The q-state clock model, which has Z_q symmetry, is a well-known discrete analog of the XY model. For the case of $q \leqslant 4$, the clock model exhibits a second-order phase transition described by the unitary minimal series of conformal field theory (CFT). If $q > 4$, the clock model has an intermediate critical phase between the high-temperature disordered phase and low-temperature ordered phase [2–5], where transitions to the critical phase are of Berezinskii-Kosterlitz-Thouless (BKT) type [6–8]. As q increases, the low-temperature ordered phase shrinks, and the $O(2)$ symmetry is finally recovered in the limit $q \to \infty$.

Discretization of the classical Heisenberg model, which has $O(3)$ symmetry, is not straightforward, in the sense that there is no established route of taking the continuous-symmetry limit. A possible manner of discretization is to introduce polyhedral anisotropies, such as tetrahedral, cubic, octahedral, icosahedral, and dodecahedral ones, which correspond to the discrete subgroups of the $O(3)$ symmetry group. Let us consider the discrete vector-spin models, where on each lattice site there is a unit vector spin that can point to the vertices of a polyhedron. The tetrahedron model can be mapped to the four-state Potts model [9]. For the octahedron model, the presence of a weak first-order phase transition was suggested by Patrascioiu and Seiler [10], and afterward was numerically confirmed [11]. The cube model can be mapped to three decoupled Ising models. Patrascioiu *et al.* reported a second-order transition for the icosahedron and dodecahedron models, respectively, which have 12 and 20 local degrees of freedom [10,12,13]. For the icosahedron model, the estimated transition temperatures is $1/T_c = 1.802 \pm 0.001$ and its critical indices are $\nu \sim 1.7$ and $\gamma \sim 3.0$, which are inconsistent with the minimal series of CFT. By contrast, Surungan *et al.* gave another estimation $\nu \simeq 1.31$ for the same transition temperature [14]. However, the system sizes of Monte Carlo simulations in previous works may be too small to conclude the universality of the icosahedron model. Finally, the possibility of an intermediate phase was suggested for the dodecahedron model in Refs. [12,13], whereas a solo second-order transition was suggested in Ref. [14].

In this article, we focus on the critical behavior of the icosahedron model. We calculate the magnetization, effective correlation length, and entanglement entropy in the bulk limit by means of the corner-transfer-matrix renormalization group (CTMRG) method [15,16], which is based on Baxter's corner-transfer-matrix (CTM) scheme [17–19]. An advantage of the CTMRG method is that we can treat sufficiently large system sizes to obtain conventional bulk physical quantities. Actually, the system size of CTM in this work is up to $10^4 \times 10^4$ sites, which can be viewed as a bulk limit in comparison with the (effective) correlation length of the system. Instead, CTMRG results are strongly dependent on m, the number of states kept for the block-spin variables, near the transition point. Nevertheless, this m dependence of CTMRG results provides a powerful tool for the scaling analysis with respect to m [20–23], the formulation of which is similar to conventional finite-size scaling analyses [24,25]. The m-scaling analysis actually extracts the presence of a second-order phase transition with the critical exponents $\nu = 1.62 \pm 0.02$ and $\beta = 0.12 \pm 0.01$. Another interesting point about the CTMRG approach is that the classical analog of entanglement entropy [26] can be straightforwardly calculated through a reduced density matrix constructed from CTMs. The m-dependence analysis of entanglement entropy also yields a central charge $c = 1.90 \pm 0.02$, which cannot be explained by the minimal series of CFT.

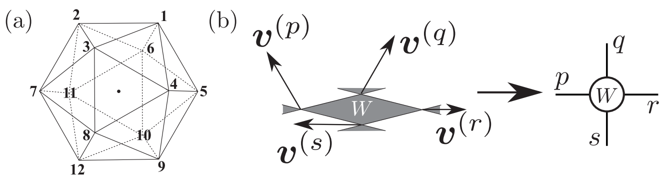

FIG. 1. (a) Numbering of the vertices of the icosahedron. (b) Local Boltzmann weight in Eq. (2) defined for a "black" plaquette, and its tensor representation.

This article is organized as follows. In the next section, we introduce the icosahedron model, and briefly explain its tensor-network representation and CTMRG method. We first show the temperature dependence of the magnetization to capture the nature of the phase transition. In Sec. III, we apply finite-m scaling to the effective correlation length, magnetization, and entanglement entropy. The transition temperature, critical exponents, and the central charge are estimated in detail. The results are summarized in the last section.

II. ICOSAHEDRON MODEL

Let us consider the icosahedron model, which is a discrete analog of the classical Heisenberg model. On each site of the square lattice, there is a vector spin $\boldsymbol{v}^{(p)}$ of unit length, which points to one of the vertices of the icosahedron, shown in Fig. 1(a), where p is the index of vertices running from 1 to 12. Figure 1(b) shows four vector spins $\boldsymbol{v}^{(p)}$, $\boldsymbol{v}^{(q)}$, $\boldsymbol{v}^{(r)}$, and $\boldsymbol{v}^{(s)}$, around a "black" plaquette, where we have introduced a chessboard pattern on the lattice. We have omitted the lattice index of these spins, since they can be formally distinguished by p, q, r, and s, which represent the directions of the spins. Neighboring spins have Heisenberg-like interaction, which is represented by the inner product between them. Thus, the local energy around the plaquette in Fig. 1(b) is written as

$$h_{pqrs} = -J(\boldsymbol{v}^{(p)} \cdot \boldsymbol{v}^{(q)} + \boldsymbol{v}^{(q)} \cdot \boldsymbol{v}^{(r)} + \boldsymbol{v}^{(r)} \cdot \boldsymbol{v}^{(s)} + \boldsymbol{v}^{(s)} \cdot \boldsymbol{v}^{(p)}). \tag{1}$$

In the following, we assume that the coupling constant is spatially uniform and ferromagnetic $J > 0$.

We represent the partition function of the system in the form of a vertex model, which can be regarded as a two-dimensional tensor network. For each black plaquette on the chessboard pattern introduced onto the square lattice, we assign the local Boltzmann weight

$$W_{pqrs} = \exp\left[\frac{h_{pqrs}}{T}\right], \tag{2}$$

where T denotes the temperature in the unit of the Boltzmann constant. Note that the vertex weight W_{pqrs} is invariant under cyclic rotations of the indices. Throughout this article we choose J as the unit of energy. As shown in Fig. 1(b), the weight W_{pqrs} is naturally interpreted as a four-leg tensor, and thus the partition function can be represented as a contraction among tensors, as schematically drawn in the right-hand side panel of Fig. 2.

In Baxter's CTM formulation, the whole lattice is divided into four quadrants [17–19], as shown in Fig. 2. The partition function of a square-shaped finite-size lattice is expressed by a trace of the fourth power of CTMs,

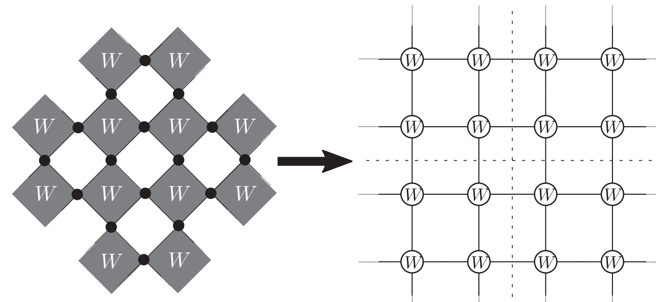

FIG. 2. Icosahedron model on the diagonal lattice, where W on each black plaquette represents the local Boltzmann weight of Eq. (2). The partition function can be represented by a tensor network on the square lattice. The dashed lines show the division of the system into quadrants corresponding to CTMs.

$$Z = \mathrm{Tr}\, C^4, \tag{3}$$

where C denotes the CTM. Note that each matrix element of C corresponds to the partition function of the quadrant where the spin configurations along the row and column edges are specified. We numerically obtain Z by means of the CTMRG method [15,16], where the area of CTM is increased iteratively by repeating the system-size extension and renormalization group (RG) transformation. Then, the matrix dimension of C is truncated with a cutoff dimension m, and under an appropriate normalization, C converges to its bulk limit after a sufficient number of iterations, even if we assume a fixed boundary condition. All the numerical data shown in this article are obtained after such a convergence. The numerical precision of CTMRG results are controlled by the cutoff m for the singular value spectrum $\{\lambda_i\}$ of CTMs with a truncation error $\epsilon(m) = 1 - \sum_{i=1}^{m} \lambda_i^4$. The universal distribution of the spectrum [27,28] suggests that the asymptotic behavior of $\epsilon(m)$ could be model independent.

In practical computations, we assume a fixed boundary condition, where all the spins are pointing to the direction $\boldsymbol{v}^{(1)}$ on the boundary of the system. We define an order parameter as the magnetization M at the center of the system,

$$M = \frac{1}{Z}\sum_{s=1}^{12}(\boldsymbol{v}^{(1)} \cdot \boldsymbol{v}^{(s)}\, \mathrm{Tr}'[C^4]), \tag{4}$$

where $\boldsymbol{v}^{(s)}$ is the vector spin at the center, and Tr' represents the partial trace except for $\boldsymbol{v}^{(s)}$. Figure 3 shows the temperature dependence of the magnetization M calculated with $m = 100$, 200, 300, 400, and 500. The magnetization is well converged with respect to m for $T < 0.55$ or $T > 0.57$, and the result supports the emergence of the ordered phase in the low-temperature region, as reported by Patrascioiu *et al.* [10,12,13]. As shown in the inset, however, the curve of M has a shoulder structure exhibiting a strong m dependence in the region $0.55 < T < 0.57$.

In order to see the nature of the observed shoulder structure in M, we calculate the probability $P^{(s)}$ of finding $\boldsymbol{v}^{(s)}$ at the center of the system. Figure 4 shows the temperature dependence of $P^{(s)}$ with $m = 500$. In the region $T < 0.55$,

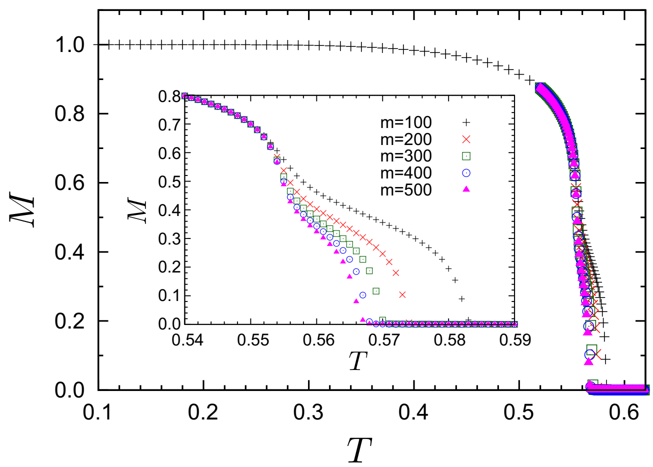

FIG. 3. Temperature dependence of magnetization M for several m. Inset: Magnified view in the region $0.54 \leqslant T \leqslant 0.59$.

the probability $P^{(1)}$ is dominant. Around $T \sim 0.56$, the values of $P^{(s)}$ for $s = 2$, 3, 4, 5, and 6 are comparable to $P^{(1)}$, and the sum $P^{(2)} + P^{(3)} + P^{(4)} + P^{(5)} + P^{(6)}$ is larger than $P^{(1)}$. Such a marginal behavior might suggest the possibility of an intermediate (or floating) critical phase, such as the two succeeding phase transitions in clocklike models [5,29–37]. We perform a scaling analysis with respect to m to clarify the nature of the phase transition in the next section.

III. SCALING ANALYSIS

As described above, the calculated results of the magnetization M exhibit a finite-m dependence near the transition point. In general, the cutoff dimension m for the CTM introduces an effective correlation length in the critical region [38,39], which corresponds to a regularization for the infrared divergence. By controlling the cutoff m, we can systematically analyze the critical behavior in the vicinity of the critical point, which we

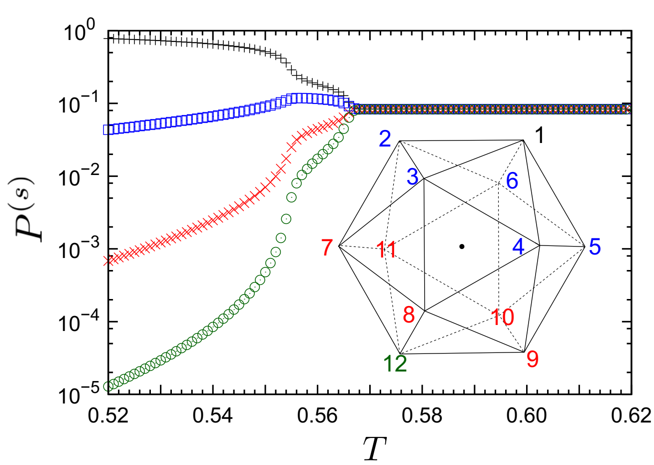

FIG. 4. Probability $P^{(s)}$ of finding $\boldsymbol{v}^{(s)}$ at the center of the system with $m = 500$. Plus marks and green circles denote $P^{(1)}$ and $P^{(12)}$, respectively. Blue squares denote $P^{(s)}$ for $s = 2$, 3, 4, 5, and 6, where these probabilities are the same. Red crosses denote $P^{(s)}$ for $s = 7$, 8, 9, 10, and 11.

call finite-m scaling [20–23], which shares many aspects with finite-size scaling analyses [24,25].

In the scaling analysis, one generally assumes that an observable A with the scaling dimension x_A obeys the following scaling function,

$$A(b,t) = b^{x_A/\nu} f_A(b^{1/\nu} t), \tag{5}$$

where $t = T/T_c - 1$ is the scaled temperature and b is a characteristic length scale intrinsic to the system, which basically corresponds to the correlation length. In the finite-size scaling analysis, b is replaced by the linear dimension of system ℓ, and then the scaling function f_A is extracted by a systematic control of ℓ. Note that the asymptotic forms $f_A(y) \sim y^{-x_A}$ for $y \gg 1$ and $f_A(y) \sim$ const for $y \to 0$ are also assumed in Eq. (5), in order to reproduce the proper scaling law in the bulk limit $\ell \to \infty$.

For finite-m scaling in CTMRG, meanwhile, we introduce a well-controllable length scale through the cutoff dimension m, instead of ℓ. After a sufficient number of iterations in CTMRG, we have a renormalized row-to-row transfer matrix. We can then define an effective correlation length

$$\xi(m,t) = [\ln(\zeta_1/\zeta_2)]^{-1}, \tag{6}$$

where ζ_1 and ζ_2 are the largest and second-largest eigenvalues of the renormalized row-to-row transfer matrix. Note that the unit of length is set as the lattice constant. An essential point is that the following scaling relation can be assumed,

$$\xi(m,t) \sim m^{\kappa} g(m^{\kappa/\nu} t), \tag{7}$$

with the asymptotic forms $g(y) \sim |y|^{-\nu}$ for $y \gg 1$ and $g(y) \sim$ const for $y \to 0$. Each limit yields the behavior $\xi(m,t) \sim t^{-\nu}$ for a finite t under the condition $m^{\kappa} \gg t^{-\nu}$, and $\xi(m,t) \sim m^{\kappa}$ for a finite m under $m^{\kappa} \ll t^{-\nu}$ [20,21]. Note that κ is an independent scaling dimension, which is characteristic of the matrix-product-state (MPS) description of the eigenvector of the row-to-row transfer matrix. Combining $b \sim \xi(m,t)$ and Eq. (5), we obtain the finite-m scaling formula as

$$A(m,t) = m^{x_A \kappa/\nu} \chi_A(m^{\kappa/\nu} t), \tag{8}$$

where χ_A is a new scaling function satisfying $\chi_A(y) \sim |y|^{-x_A}$ for $y \gg 1$. For a finite t under the condition $m^{\kappa/\nu} t \gg 1$, Eq. (8) reproduces $A(m,t) \sim |t|^{-x_A}$, while for a finite m under $m^{\kappa/\nu} t \ll 1$, Eq. (8) gives $A(m,t) \sim m^{-\kappa x_A/\nu}$.

We apply the scaling analysis to several quantities calculated by CTMRG, with the help of a Bayesian analysis for fitting [40]. We consider the temperature region $0.520 \leqslant T \leqslant 0.619$ for $m = 100$, 200, 300, 400, and 500 in the following scaling analysis. We first apply the analysis to $\xi(m,t)$ in Eq. (6) and estimate the critical temperature T_c, and exponents κ and ν. Figure 5(a) shows the scaling plot of $\xi(m,t)$ with the best fit values, $T_c = 0.555\,048(43)$, $\nu = 1.617(13)$, and $\kappa = 0.8983(17)$, where all data collapse on the scaling function g in Eq. (7). The fitting errors in the Bayesian analysis are shown in the parentheses. If we use the data for $200 \leqslant m \leqslant 500$, we obtain $T_c = 0.554\,940(42)$, $\nu = 1.623(13)$, and $\kappa = 0.8830(19)$. Comparing these two fitting results, we adopt $T_c = 0.5550 \pm 0.0001$, $\nu = 1.62 \pm 0.02$, and $\kappa = 0.89 \pm 0.02$. This result of T_c is consistent with the values $T_c \simeq 0.555$ reported by both Patrascioiu *et al.* [10,12,13] and Surungan *et al.* [14]. While the critical exponent ν is

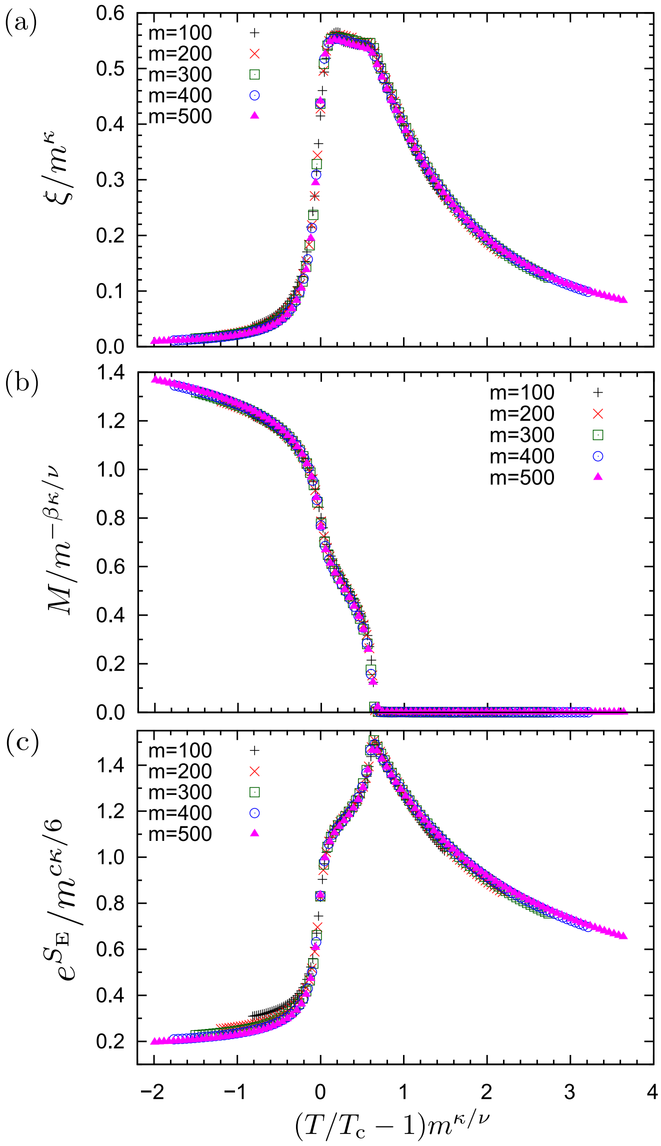

FIG. 5. Finite-m scalings for (a) correlation length in Eq. (6), (b) magnetization M in Eq. (4), and (c) entanglement entropy in Eq. (10).

consistent with the value $\nu = 1.7^{+0.3}_{-0.1}$ in Refs. [10,12,13], it has a discrepancy from $\nu = 1.31 \pm 0.01$ in Ref. [14].

On the basis of the above T_c, ν, and κ, moreover, we perform a finite-m scaling analysis for the magnetization M shown in Fig. 3. A particular point is that the shoulder structure in the inset of Fig. 3 directly reflects on the scaling function of Fig. 5(b). Moreover, such shoulder structures of the scaling functions are consistently observed in Figs. 5(a) and 5(c). These behaviors imply that the transition of the icosahedron model is described by a solo second-order transition, unlike the clock models of $q > 4$ where an intermediate critical region emerges. Using the Bayesian fitting, then, we obtain $\beta = 0.1293(27)$ for $m = 100$–500 and $\beta = 0.1234(33)$ for $m = 200$–500. Taking into account the discrepancy, we adopt $\beta = 0.12 \pm 0.01$. We, however, think that this value should be improved in further extensive calculations.

In order to obtain additional information for the scaling universality, we calculate the classical analog of the entanglement entropy. The concept of entanglement can be introduced to two-dimensional statistical models through quantum-classical correspondence [41–44]. Then, an essential point is that the fourth power of CTM, which appears in Eqs. (3) and (4), can be interpreted as a density matrix of the corresponding one-dimensional quantum system [45]. From the normalized density matrix

$$\rho = \frac{C^4}{Z}, \tag{9}$$

we obtain the classical analog of entanglement entropy, in the form of von Neumann entropy [46,47],

$$S_{\rm E} = -\mathrm{Tr}\,\rho \ln \rho. \tag{10}$$

In the context of CTMRG, the following relation,

$$S_{\rm E}(m,t) \sim \frac{c}{6} \ln \xi(m,t) + \mathrm{const}, \tag{11}$$

is satisfied around the criticality [48,49], where c is the central charge. Taking the exponential of both sides of this equation, and substituting Eq. (7), we obtain

$$e^{S_{\rm E}} \sim a[\xi(m,t)]^{c/6} = a[m^{\kappa} g(m^{\kappa/\nu} t)]^{c/6} = m^{c\kappa/6} \tilde{g}(m^{\kappa/\nu} t), \tag{12}$$

where a is a nonuniversal constant, and $\tilde{g} \equiv a g^{c/6}$. Thus the critical exponent for $e^{S_{\rm E}}$ is identified as $c\nu/6$.

Using T_c, κ, and ν previously obtained by the finite-m scaling for $\xi(m,t)$, we can estimate the central charge c. Figure 5(c) shows the scaling plot of Eq. (12) for the data of $m = 100$, 200, 300, 400, and 500. The central charge is estimated as $c = 1.894(12)$. If we exclude the case $m = 100$ for the scaling analysis, we obtain $c = 1.900(15)$. Considering the discrepancy between the above values of c, we adopt $c = 1.90 \pm 0.02$.

Here, it should be noted that this value is consistent with the relation

$$\kappa = \frac{6}{c(\sqrt{12/c} + 1)}, \tag{13}$$

which is derived from the MPS description of a one-dimensional critical quantum system [22]. Substituting $c = 1.90$ and $\kappa = 0.89$ into Eq. (13), we actually have $6/\{c(\sqrt{12/c} + 1)\} - \kappa = 0.009$, which provides a complementary check of the finite-m scaling in CTMRG.

IV. SUMMARY AND DISCUSSION

We have investigated the phase transition and its critical properties of the icosahedron model on a square lattice, where the local vector spin has 12 degrees of freedom. We have calculated the magnetization, the effective correlation length, and the classical analog of entanglement entropy by means of the CTMRG method. The CTMRG results are strongly dependent on m, which is the cutoff dimension of CTMs, near the critical point. We have then performed a finite-m scaling analysis and found that the numerical data can be well fitted with the scaling functions, including the shoulder structures. We have thus confirmed that the icosahedron model exhibits a second-order phase transition at $T_c = 0.5550 \pm 0.0001$, below which the icosahedral symmetry is broken to a fivefold axial symmetry. Also, the scaling exponents are estimated as $\nu = 1.62 \pm 0.02$, $\kappa = 0.89 \pm 0.02$, and $\beta = 0.12 \pm 0.01$. From the relation between entanglement entropy and the effective correlation length, moreover, we have extracted the central charge as $c = 1.90 \pm 0.02$, which cannot be described by the minimal series of CFT. The clarification of the mechanism of such a nontrivial critical behavior in the icosahedron model is an important future issue.

Our original motivation was from a systematical analysis of the continuous-symmetry limit toward the $O(3)$ Heisenberg spin. In this sense, the next target is a dodecahedron model having 20 local degrees of freedom, which requires massive parallelized computations of CTMRG. In addition, it is an interesting problem to introduce XY-like uniaxial anisotropy to the icosahedron and dodecahedron models. A crossover of universality between the icosahedron/dodecahedron model and the clock models can be expected, where the shoulder structures of the scaling functions may play an essential role.

ACKNOWLEDGMENTS

This research was partially supported by Grants-in-Aid for Scientific Research under Grants No. 25800221, No. 26400387, No. 17H02931, and No. 17K14359 from JSPS and by VEGA 2/0130/15 and APVV-16-0186. It was also supported by MEXT as "Challenging Research on Post-K computer" (Challenge of Basic Science: Exploring the Extremes through Multi-Physics Multi-Scale Simulations). The numerical computations were performed on the K computer provided by the RIKEN Advanced Institute for Computational Science through the HPCI System Research project (Project ID hp160262).

[1] N. D. Mermin and H. Wagner, Phys. Rev. Lett. **17**, 1133 (1966).
[2] S. Elitzur, R. B. Pearson, and J. Shigemitsu, Phys. Rev. D **19**, 3698 (1979).
[3] K. Nomura, J. Phys. A **39**, 2953 (2006).
[4] G. Ortiz, E. Cobanera, and Z. Nussinov, Nucl. Phys. B **854**, 780 (2012).
[5] Y. Kumano, K. Hukushima, Y. Tomita, and M. Oshikawa, Phys. Rev. B **88**, 104427 (2013).
[6] V. L. Berezinskii, Sov. Phys. JETP **32**, 493 (1971).
[7] V. L. Berezinskii, Sov. Phys. JETP **34**, 610 (1972).
[8] J. M. Kosterlitz and D. J. Thouless, J. Phys. C **6**, 1181 (1973).
[9] F. Y. Wu, Rev. Mod. Phys. **54**, 235 (1982).
[10] A. Patrascioiu and E. Seiler, Phys. Rev. D **64**, 065006 (2001).
[11] R. Krčmár, A. Gendiar, and T. Nishino, Phys. Rev. E **94**, 022134 (2016).
[12] A. Patrascioiu, J.-L. Richard, and E. Seiler, Phys. Lett. B **241**, 229 (1990).
[13] A. Patrascioiu, J.-L. Richard, and E. Seiler, Phys. Lett. B **254**, 173 (1991).
[14] T. Surungan and Y. Okabe, in *Proceedings of 3rd JOGJA International Conference on Physics* (Gadjah Mada University, Yogyakarta, 2012), pp. 65–69; arXiv:1709.03720.
[15] T. Nishino and K. Okunishi, J. Phys. Soc. Jpn. **65**, 891 (1996).
[16] T. Nishino and K. Okunishi, J. Phys. Soc. Jpn. **66**, 3040 (1997).
[17] R. J. Baxter, J. Math. Phys. **9**, 650 (1968).
[18] R. J. Baxter, J. Math. Phys. **19**, 461 (1978).
[19] R. J. Baxter, *Exactly Solved Models in Statistical Mechanics* (Academic, London, 1982).
[20] T. Nishino, K. Okunishi, and M. Kikuchi, Phys. Lett. A **213**, 69 (1996).
[21] L. Tagliacozzo, T. R. de Oliveira, S. Iblisdir, and J. I. Latorre, Phys. Rev. B **78**, 024410 (2008).
[22] F. Pollmann, S. Mukerjee, A. M. Turner, and J. E. Moore, Phys. Rev. Lett. **102**, 255701 (2009).
[23] B. Pirvu, G. Vidal, F. Verstraete, and L. Tagliacozzo, Phys. Rev. B **86**, 075117 (2012).
[24] M. E. Fisher and M. N. Barbe, Phys. Rev. Lett. **28**, 1516 (1972).
[25] M. N. Barber, in *Phase Transitions and Critical Phenomena*, edited by C. Domb and J. L. Lebowitz (Academic, New York, 1983), Vol. 8.
[26] C. H. Bennett, H. J. Bernstein, S. Popescu, and B. Schumacher, Phys. Rev. A **53**, 2046 (1996).
[27] K. Okunishi, Y. Hieida, and Y. Akutsu, Phys. Rev. E **59**, R6227 (1999).
[28] P. Calabrese and A. Lefevre, Phys. Rev. A **78**, 032329 (2008).
[29] J. Tobochnik, Phys. Rev. B **26**, 6201 (1982); **27**, 6972 (1983).
[30] M. S. S. Challa and D. P. Landau, Phys. Rev. B **33**, 437 (1986).
[31] A. Yamagata and I. Ono, J. Magn. Magn. Mater. **90-91**, 293 (1990); J. Phys. A **24**, 265 (1991).
[32] Y. Tomita and Y. Okabe, Phys. Rev. B **65**, 184405 (2002).
[33] C.-O. Hwang, Phys. Rev. E **80**, 042103 (2009).
[34] A. F. Brito, J. A. Redinz, and J. A. Plascak, Phys. Rev. E **81**, 031130 (2010).
[35] S. K. Baek, P. Minnhagen, and B. J. Kim, Phys. Rev. E **81**, 063101 (2010).
[36] S. K. Baek, H. Mäkelä, P. Minnhagen, and B. J. Kim, Phys. Rev. E **88**, 012125 (2013).
[37] R. Krčmár, A. Gendiar, and T. Nishino, arXiv:1612.07611.
[38] S. K. Tsang, J. Stat. Phys. **20**, 95 (1979).
[39] C. Liu, L. Wang, A. W. Sandvik, Y.-C. Su, and Y.-J. Kao, Phys. Rev. B **82**, 060410(R) (2010).
[40] K. Harada, Phys. Rev. E **84**, 056704 (2011).
[41] E. Fradkin and L. Susskind, Phys. Rev. D **17**, 2637 (1978).
[42] H. F. Trotter, Pac. J. Math. **8**, 887 (1958), https://projecteuclid.org/euclid.pjm/1103039709.
[43] M. Suzuki, J. Phys. Soc. Jpn. **21**, 2274 (1966).
[44] M. Suzuki, Prog. Theor. Phys. **56**, 1454 (1976).
[45] H. Ueda, K. Okunishi, and T. Nishino, Phys. Rev. B **89**, 075116 (2014).
[46] J. von Neumann, Nachr. Ges. Wiss. Goettingen, Math.-Phys. Kl. **1**, 273 (1927).
[47] J. von Neumann, *Mathematische Grundlagen der Quantenmechanik* (Springer, Berlin, 1932).
[48] G. Vidal, J. I. Latorre, E. Rico, and A. Kitaev, Phys. Rev. Lett. **90**, 227902 (2003).
[49] P. Calabrese and J. Cardy, J. Stat. Mech. (2004) P06002.